

# Shape-centered Representation Learning for Visible-Infrared Person Re-identification

Shuang Li, Jiayu Leng, Ji Gan, Mengjingcheng Mo, and Xinbo Gao, *Senior Member, IEEE*

**Abstract**—Current Visible-Infrared Person Re-Identification (VI-ReID) methods prioritize extracting distinguishing appearance features, ignoring the natural resistance of body shape against modality changes. Initially, we gauged the discriminative potential of shapes by a straightforward concatenation of shape and appearance features. However, two unresolved issues persist in the utilization of shape features. One pertains to the dependence on auxiliary models for shape feature extraction in the inference phase, along with the errors in generated infrared shapes due to the intrinsic modality disparity. The other issue involves the inadequately explored correlation between shape and appearance features. To tackle the aforementioned challenges, we propose the Shape-centered Representation Learning framework (ScRL), which focuses on learning shape features and appearance features associated with shapes. Specifically, we devise the Shape Feature Propagation (SFP), facilitating direct extraction of shape features from original images with minimal complexity costs during inference. To reconstitute inaccuracies in infrared body shapes at the feature level, we present the Infrared Shape Restitution (ISR). Furthermore, to acquire appearance features related to shape, we design the Appearance Feature Enhancement (AFE), which accentuates identity-related features while suppressing identity-unrelated features guided by shape features. Extensive experiments are conducted to validate the effectiveness of the proposed ScRL. Achieving remarkable results, the Rank-1 (mAP) accuracy attains 76.1%, 71.2%, 92.4% (72.6%, 52.9%, 86.7%) on the SYSU-MM01, HITSZ-VCM, RegDB datasets respectively, outperforming existing state-of-the-art methods.

**Index Terms**—person re-identification, logical relation inference, multi-view information interaction, domain adaptation.

## I. INTRODUCTION

Person Re-Identification (ReID) serves the purpose of identifying specific individuals across non-overlapping camera views, carrying substantial significance in the domain of intelligent surveillance systems. Consequently, it has garnered considerable attention from a multitude of researchers, undergoing rapid advancements in recent times [1]–[7]. However, the majority of existing methods are confined to scenarios

This work was supported in part by the National Natural Science Foundation of China under Grants No. 62102057, No. U22A2096, and No. 62221005, in part by the National Science Foundation of Chongqing under Grant No. CSTB2022NSCQ-MSX1024, in part by the Science and Technology Research Program of Chongqing Municipal Education Commission under Grant No. KJZD-K202300604, in part by the Chongqing Postdoctoral Innovative Talent Plan under Grant No. CQBX202217, in part by the Postdoctoral Science Foundation of China under Grant No. 2022M720548, in part by the Chongqing Institute for Brain and Intelligence, and in part by Chongqing Excellent Scientist Project under Grant No. cstc2021ycjh-bgzxm0339. (Corresponding author: X. Gao.)

S. Li, J. Leng, J. Gan, M. Mo and X. Gao, are with the Chongqing University of Posts and Telecommunications, Chongqing, China (E-mail: shuangli936@gmail.com, lengjx@cqupt.edu.cn, ganji@cqupt.edu.cn, mo1031@live.com, gaobx@cqupt.edu.cn).

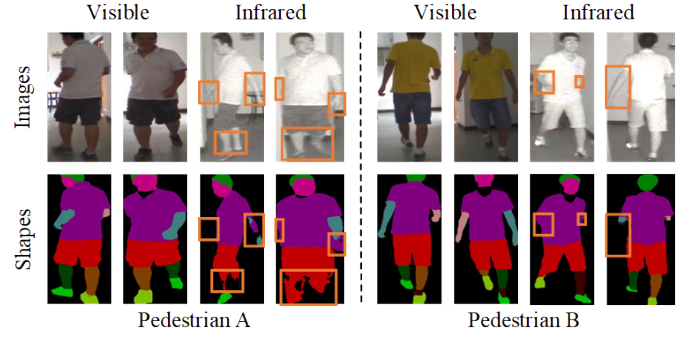


Fig. 1. The visible (infrared) images and their corresponding body shapes and the orange box indicate an incorrect area of the infrared body shape.

where pedestrians are solely present during daylight hours [8]–[14]. Consequently, the efficacy of these approaches hinges on visible appearances. This limitation has resulted in notable performance degradation when attempting to match pedestrians captured by both visible (VIS) and infrared (IR) cameras. To effectively tackle this issue, the Visible-Infrared Person Re-Identification (VI-ReID) task [15] was introduced. This task aims to enable the retrieval of pedestrians across the distinct spectra of IR and VIS [16], [17]. In contrast to the extensively explored realm of ReID within the visible spectrum, the domain of VI-ReID presents notably greater challenges. This is primarily attributed to substantial intra- and inter-modality variations that exist between images captured in the visible (VIS) and infrared (IR) spectra.

A prevailing trend among existing VI-ReID methods is the zealous pursuit of mining modality-shared appearance cues to enhance the discriminability of features but ignoring the learning of body shape clues. Nevertheless, three compelling reasons underscore the importance of not disregarding body shape cues. **1)** The natural resistance of body shape to modality changes stands as the first reason. As illustrated in Fig. 1, no modality discrepancy in the body shape corresponding to infrared and visible images. **2)** The second rationale stems from the identity-discriminative nature of body shape. As depicted in Fig. 1, one can observe that pedestrian A slightly fatter than pedestrian B in terms of their global body shapes, with distinctions extending to local characteristics such as facial shape, hair shape, limb shape, etc. Thus, the identification of pedestrians becomes feasible through body shape analysis, even when changes in modality render color texture features unreliable. **3)** Body shape estimation can be achieved through

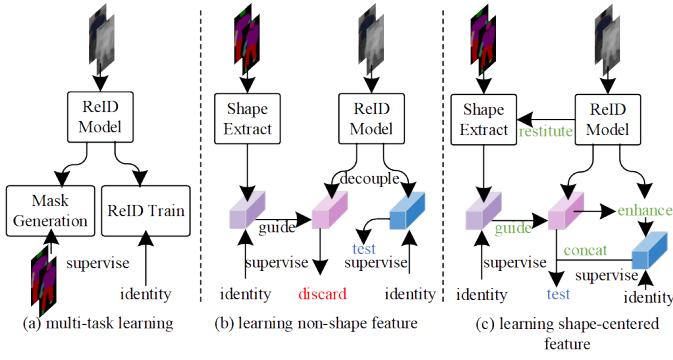


Fig. 2. Framework comparison of VI-ReID methods that explore the utilization of body shape. (a) Learning the features associated with shapes through multi-task learning. (b) Learning diverse appearance features through decoupling and discarding shape features. (c) Learning shape features and enhancing appearance features through shape features.

pre-trained human parsing models, obviating the necessity for human annotation. Moreover, single-modality ReID methods have demonstrated successful instances in this regard.

Nevertheless, when attempting to apply body shape estimates to the VI-ReID task, as depicted in Fig. 1, certain inaccuracies become evident in the infrared body shapes associated with infrared images. These inaccuracies manifest as discrepancies such as missing or inaccurately represented local shapes, with a predominant focus on limbs. This occurrence stems from the skin color of pedestrians bearing a striking resemblance to the background color present in infrared images. Consequently, the human parsing model erroneously categorizes exposed arms and legs as the background. Although the identity-related information carried by body shapes indeed falls within the realm of modality-shared cues, the presence of incorrect infrared body shapes limits the effective utilization of these cues. Furthermore, we acknowledge that the discriminative cues offered by body shape possess limitations. Depending solely on body shape for the identification of all pedestrians proves inadequate. Compared to the body shape, VIS (IR) pedestrian images contain richer identity clues, including clothing style, hairstyle, and more [18]. However, the direct extraction of the aforementioned appearance features from images presents challenges due to the interference caused by modality-specific information (color features in visible images, temperature in infrared images) and intricate backgrounds. Based on our observations, these appearance features exhibit a strong correlation with body shape, while the modality-specific information and background are unrelated to the body shape. **So effectively utilizing body shape not only requires extracting discriminant shape features from the visible (infrared) images but also requires effectively exploring the correlation between shape features and pedestrian appearance features.**

Within the realm of VI-ReID, two methods closely aligned with body shape considerations are CMMTL [18] and SEFL [19]. Illustrated in Fig. 2, CMMTL undertakes the implicit acquisition of shape features, leveraging human parsing as an auxiliary task. However, it falls short in addressing the

potential adverse effects of incorrect infrared shape representation and fails to elucidate the manner in which shape features contribute to enhancement, thus lacking interpretability. On the other hand, SEFL adopts the stance that body shape cues are unreliable and subsequently seeks to acquire diverse modality-shared features by disentangling and discarding potentially unreliable shape features. In contrast, our approach diverges from SEFL’s viewpoint. We contend that body shape features possess intrinsic discriminative qualities and are adept at withstanding modality variations. Consequently, our focus centers on devising effective strategies for acquiring robust body shape features and delving into the intricate relationship between these features and appearance features.

Based on the aforementioned insights and analysis, we introduce the Shape-centered Representation Learning (ScRL) framework, which facilitates the direct acquisition of modality-shared shape features and shape-associated appearance features from visible (infrared) images. Illustrated in Fig. 3, this proposed framework comprises three key components: Infrared Shape Restitution (ISR), Shape Feature Propagation (SFP), and Appearance Feature Enhancement (AFE). Specifically, ISR is designed to reconstitute IR shapes by capturing missing infrared shape features from appearance features during the training phase. SFP is designed to make the model can directly extract shape features from pedestrian images without the participation of additional auxiliary networks during the inference phase by transferring the ability of the shape features extraction to the appearance feature extraction network in the training phase. AFE is aimed at mining appearance features associated with body shape by introducing a two-stage cascade attention mechanism that directly and indirectly emphasizes identity-related features and suppresses identity-unrelated features.

Our main contributions are summarized as follows:

- We propose a novel deep-learning framework that prioritizes learning shape-centered features without the necessity of auxiliary networks during the inference phase. Notably, we are the first to effectively incorporate explicit shape features into VI-ReID.
- We design the Infrared Shape Resolution (ISR), which effectively restitutes erroneous infrared body shapes generated by human parsing networks and improves the discriminability of shape features.
- We design the Appearance Feature Enhancement (AFE) to elevate appearance features by harnessing the inherent relationship between shape and appearance features.
- Extensive experimental results on SYSU-MM01, RegDB, and HITSZ-VCM datasets show the proposed ScRL achieves a new state-of-the-art performance.

The rest of this paper is organized as follows. Section II introduces related work; Section III elaborates the proposed method; Section IV analyzes the comparative experimental results; and Section V concludes this paper.

## II. RELATED WORK

### A. Visible Person Re-Identification

Visible Person Re-Identification (ReID) aims to match visible pedestrian images with the same identity under non-

overlapping cameras. With the introduction of large-scale datasets [20], [21], [22], Visible person ReID based on deep learning has rapidly developed. In order to directly conduct end-to-end training in the expected embedding space, [23] improved the hard sample mining of the classic triplet loss, which improved the discriminability of pedestrian features. In order to obtain fine-grained discriminative features, PCB [24] proposes to horizontally divide pedestrian feature maps into 6 parts to learn part-level features. MGN [25] proposes an end-to-end multi-branch deep network to learn pedestrian feature representations of different granularity. To overcome the information loss caused by convolution and pooling operations, TransReid [26] proposes a transformer-based reid framework. In addition, changes in illumination, pose, and perspective also pose challenges for extracting discriminative pedestrian features. In response to the issue of illumination changes, IID [27] proposes to eliminate the adverse effects of illumination changes by decoupling illumination features and identity features. In order to align with the standard posture of pedestrians, PIE [28] introduces the PoseBox structure to obtain pose-invariant embedded features. In response to the adverse impact of camera style changes on pedestrian matching, Camstyle [29] proposed using CycleGAN [30] to achieve transfer between different camera styles, smoothing out camera style differences at the data level.

### B. Visible-Infrared Person Re-Identification

In order to match pedestrians from different modalities, researchers have contributed a lot of excellent work, VI-ReID methods can be roughly divided into two main categories: feature-level modality alignment and image-level modality alignment methods.

The feature-level modality alignment methods aim to learn modality-shared features by aligning IR and VIS features at the feature level. HSME [31] maps features of different modalities to a unified hypersphere. MBCE [32] proposes a memory-based prototype feature learning method to suppress the modality discrepancy. MRCN [33] reduces the modality discrepancy by decoupling the modality-relevant and modality-irrelevant features. To more effectively mine diverse cross-modality clues, MPANet [34] be designed to discover the nuanced modality-shared features. DEEN [35] enhances the embedding representation in the embedding space by generating diverse embeddings.

The image level modality alignment methods alleviate modality differences by generating images with the target or intermediate modality styles. D<sup>2</sup>RL [36] transfers the style of IR (VIS) images to VIS (IR) images through the GAN network, compensating for the missing modality information. XIV [37] transform IR and VIS images into auxiliary X-modality images respectively, and perform X-IR-VIS three-mode learning. SMCL [38] generates syncretic modality images that contain information from both modalities to steer modality-invariant feature learning. However, the modality-shared clues (like shape-centered clues) have not been fully explored, which limits the discriminability of features.

### C. Semantic Parsing for Person Re-Identification

SPReID [39] first introduced human semantic parsing into the ReID to obtain refined local features. MGCAM [40] introduces human semantic parsing for the first time to construct RGB mask pairs to eliminate the adverse effects of background noise. EaNet [41] guides the ReID model through human parsing as labels for multitasking learning. In addition to the human parts captured by human parsing results, there are also some other useful clues (such as personal belongings.). P2Net [42] and ISP [43] explore more comprehensive features through accurate human parts and non-human parts. Considering that widely studied methods overly rely on color appearance and fail to apply to cloth changing ReID, FSAM [44] transfers knowledge from shape stream to appearance stream by interactive mutual learning. In the VI-ReID task, CMMTL [18] and SEFL [19] involve human semantic parsing. CMMTL uses the body shape as the semantic label guidance model to perform both VI-ReID and human semantic segmentation tasks. SEFL [19] discards the shape feature and focuses on learning identity-related modality-shared features through disentanglement learning.

Compared to their work, our method aims to learn shape-centered feature representation guided by body shape, while considering the unreliable situation of IR human semantic parsing.

## III. THE PROPOSED METHOD

### A. Preliminaries and Baseline

**Preliminaries.** Let  $X = \{(x_i^{vis}, x_i^{ir}, x_{s,i}^{vis}, x_{s,i}^{ir}, y_i) |_{i=1}^N\}$  represent the training dataset, where  $N$  represents the total number of pedestrian images,  $y_i \in \{1, 2, \dots, K\}$  represents its corresponding identity label,  $K$  represents the total number of identities.  $x_i^{vis}(x_i^{ir})$  represents the  $i$ -th VIS(IR) image,  $x_{s,i}^{vis}(x_{s,i}^{ir})$  represents the body shape corresponding to  $x_i^{vis}(x_i^{ir})$ , which is obtained by feeding  $x_i^{vis}(x_i^{ir})$  into the pre-trained Self-Correction Human Parsing (SCHP) [45] model.

**Baseline: Appearance Feature Learning.** Referring to the ReID framework named AGW [46], we adopted a dual stream network that removed the Non-local Attention as the Baseline. Specifically, a dual stream network consists of two parallel convolutional layers with unshared parameters, four blocks with shared parameters, and a Generalized-mean (GeM) Pooling layer, named  $F_a$ . Two parallel convolutional layers independently process VIS and IR images to extract low-level features, then the features are fed to the subsequent four blocks to extract high-level features  $f_i^m$ . The above process can be formalized as:

$$f_i^m = F_a(x_i^m) \quad m = \{vis, ir\}. \quad (1)$$

To ensure the identity discriminability of  $f_i^m$ , Cross Entropy (CE) loss  $L_{id}$  and Weighted Regularization Triplet (WRT) [47] loss  $L_{wrt}$  was adopt to constrain it as follows:

$$L_{id} = -\frac{1}{n_b} \sum_{i=1}^{n_b} q_i \log(W_{id}(f_i^m)) \quad , \quad (2)$$

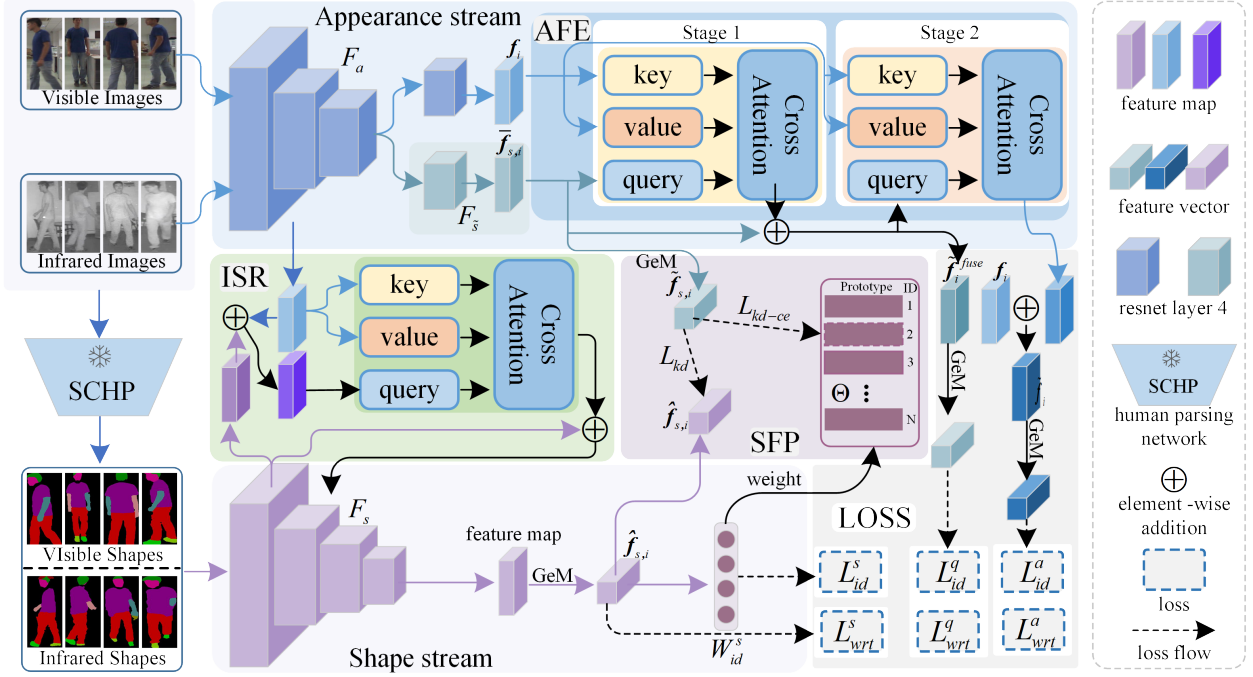


Fig. 3. Overview of our method. This framework mainly consists of Shape Feature Propagation (SFP), Infrared Shape Restitution (ISR), and Appearance Feature Enhancement (AFE), which can also be divided into appearance stream and shape stream. SFP is used to transfer the shape feature extraction ability to the appearance stream, enabling the model to directly extract shape features from the original image.

where  $n_b$  represents the batch size,  $\mathbf{W}_{id}$  represents the shared identity classifier for IR and VIS pedestrian features,  $q_i \in \mathbb{R}^{K \times 1}$  is a one-hot vector, and only the element at  $y_i$  is 1.

$$L_{wrt} = \frac{1}{n_b} \sum_{i=1}^{n_b} \log(1 + \exp(\sum_{i,j} w_{i,j}^p \mathbf{d}_{i,j}^p - \sum_{i,k} w_{i,k}^n \mathbf{d}_{i,k}^n)), \quad (3)$$

$$w_{i,j}^p = \frac{\exp(\mathbf{d}_{i,j}^p)}{\sum_{\mathbf{d}_{i,j} \in P_i} \exp(\mathbf{d}_{i,j}^p)}, w_{i,k}^n = \frac{\exp(-\mathbf{d}_{i,k}^n)}{\sum_{\mathbf{d}_{i,k} \in N_i} \exp(-\mathbf{d}_{i,k}^n)}$$

where  $j, k$  ( $P_i, N_i$ ) represents the index of the positive and negative samples(set) corresponding to the anchor sample  $x_i$  within a batch size, respectively. And  $d_{i,j}$  represents the euclidean distance between two features:  $d_{i,j} = \|\mathbf{f}_i^m - \mathbf{f}_j^n\|_2$ .

### B. Shape Feature Learning

Although the design of the dual stream network is aimed at extracting modality-shared features, it focuses on learning pedestrian appearance features and lacks the ability to learn pedestrian body shape features. Compared to appearance features, the body shape features of pedestrians are more robust against modality changes. Therefore, in this section, we aim to learn the body shape features by the SCHP and a shape feature learning network  $F_s$ . In order to obtain discriminative body shape features, we feed the body shape  $x_{s,i}^{vis}$  and  $x_{s,i}^{ir}$  generated by the SCHP to  $F_s$  to extract the shape features  $\mathbf{f}_{s,i} = F_s(x_{s,i})$ . Then,  $\mathbf{f}_{s,i}$  is into the shape identity classifier  $\mathbf{W}_s$  for identity classification.

**Infrared Shape Restitution:** as discussed in the introduction and shown in Fig.1, inherent errors are present within the IR body shapes, which not only leads to the inability of  $F_s$  to derive adequately discriminative shape features from input

IR shapes but also limit the ability of  $F_s$  to extract VIS shape features due to pulling the distance between incorrect IR shape features and VIS shape features.

To address this issue, we propose to obtain absent shape details of the IR body shape from the corresponding IR image to reconstitute the IR shape at the feature level, as shown in Fig. 4. This module is motivated by the fact that, despite certain errors in the infrared shape generated by SCHP, the original infrared pedestrian image still contains the complete shape information. Specifically, let the IR shape feature map and IR feature map output from the  $j$ -th block of  $F_s$  and  $F_a$  be represented as  $\mathbf{f}_{s,i}^{ir,j}$  and  $\mathbf{f}_i^{ir,j}$ , respectively. In order to search for features related to incorrect IR shape in IR feature map  $\mathbf{f}_i^{ir,j}$ , we design a cross-attention consisting of query  $Q$ , key  $K$ , value  $V$ , inspired by self-attention [48]. A noteworthy distinction from self-attention is that our query is obtained by adding the IR shape feature map  $\mathbf{f}_i^{ir,j}$  and IR feature map  $\mathbf{f}_{s,i}^{ir,j}$ :

$$Q = \mathbf{W}_q(\mathbf{f}_i^{ir,j} + \mathbf{f}_{s,i}^{ir,j}), \quad (4)$$

Where  $\mathbf{W}_q$  represents the 2D convolution layer with kernel sizes of  $1 \times 1$ . The query generated by this operation contains the information required to reconstitute the body shape, so it can be used to search for valid information in the value. And the key and value are represented as:

$$K = \mathbf{W}_k(\mathbf{f}_i^{ir,j}), V = \mathbf{W}_v(\mathbf{f}_i^{ir,j}), \quad (5)$$

Where  $\mathbf{W}_k$  and  $\mathbf{W}_v$  represent the 2D convolution layer with kernel sizes of  $1 \times 1$ , respectively. Then we obtain the required feature from  $V$  and the corrected IR shape feature map  $\hat{\mathbf{f}}_{s,i}^{ir,j}$

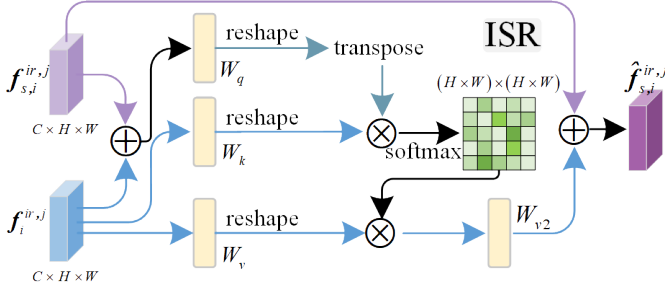


Fig. 4. Illustration of our proposed ISR that is used to obtain missing shape features from appearance features for restituting IR shapes.

can be obtained as follows:

$$\hat{f}_{s,i}^{ir,j} = W_{v2}(BN(Norm(QK^T)V)) + f_{s,i}^{ir,j}, \quad (6)$$

Where  $W_{v2}$  represents the 2D convolution layer with kernel sizes of  $1 \times 1$ ,  $BN$ ,  $Norm$  and  $(\cdot)^T$  represents the batch normalization layer, the normalization operation and the transpose operation. Following the above steps, we incorporated the infrared shape restitution attention following the first and second blocks of  $F_s$ . In order to guide the training of  $F_s$  and ISR, we introduce CE loss and WRT loss to constrain the shape features  $\hat{f}_{s,i}$  output from  $F_s$  with GeM pooling layer:

$$L_{id}^s = -\frac{1}{n_b} \sum_{i=1}^{n_b} q_i \log(W_{id}^s(\hat{f}_{s,i})), \quad (7)$$

where  $W_{id}^s$  represents the shared identity classifier for IR and VIS pedestrian shape features.

$$L_{wrt}^s = \frac{1}{n_b} \sum_{i=1}^{n_b} \log(1 + \exp(\sum_{i,j} w_{i,j}^{s,p} d_{i,j}^{s,p} - \sum_{i,k} w_{i,k}^{s,n} d_{i,k}^{s,n})), \quad (8)$$

$$w_{i,j}^{s,p} = \frac{\exp(d_{i,j}^{s,p})}{\sum_{d_{i,j} \in P_i^s} \exp(d_{i,j}^{s,p})}, w_{i,k}^{s,n} = \frac{\exp(-d_{i,k}^{s,n})}{\sum_{d_{i,k} \in N_i^s} \exp(-d_{i,k}^{s,n})}$$

where  $j, k$  ( $P_i^s, N_i^s$ ) represents the index of the positive and negative samples(set) corresponding to the anchor shape feature  $\hat{f}_{s,i}$  within a batch size, respectively. And  $d_{i,j}^s$  represents the euclidean distance between two shape features:  $d_{i,j}^s = \|\hat{f}_{s,i} - \hat{f}_{s,j}\|_2$ . Importantly, it should be highlighted that the VIS shape features do not require restitution and we mix them with corrected IR shape features in batch size to participate in the loss calculation. Therefore, the VIS shape features can guide the learning of the ISR at the loss level.

**Shape Feature Propagation:** we can obtain shape features through the collaboration of appearance feature extraction network  $F_a$ , shape feature learning network  $F_s$ , and ISR. However, this poses challenges to model deployment due to the increased parameters and computational complexity. Therefore, it is crucial to transfer the ability of extracting shape features to the appearance stream network, so that the testing phase does not require the participation of the shape stream network.

Towards this objective, we replicate the fourth block of  $F_a$  as the shape subnetwork  $F_s$  with GeM pooling layer and apply it to the output features of the third block of  $F_a$  to obtain the

shape features  $\tilde{f}_{s,i}$  under the guidance of the shape features  $\hat{f}_{s,i}$  output from the  $F_s$  at instance (Eq.9) and prototype level (Eq.10).

$$L_{kd} = \frac{1}{n_b} \sum_{i=1}^{n_b} \|\tilde{f}_{s,i} - \hat{f}_{s,i}\|_2, \quad (9)$$

where  $n_b$  represents the batch size, and  $\|\cdot\|_2$  represents  $l_2$ -norm.

$$L_{kd\_ce} = -\frac{1}{n_b} \sum_{i=1}^{n_b} q_i \log(\tilde{f}_{s,i} \Theta^T), \quad (10)$$

where  $\Theta \in \mathbb{R}^{C \times K}$  represents the class prototype from the classifier  $W_{id}^s$ .

### C. Appearance Feature Enhancement

In addition to shape features, pedestrian appearance contains essential identity cues like clothing style, hairstyle and etc. Extracting these features from the original image is complex due to modality(background) changes. It is worth noting that these clues are tied to body shape—hairstyle features relate to head shape. Therefore, we expect to mine these appearance clues mentioned above and suppress identity-unrelated modality-specific features, such as color, temperature, etc. Due to the limited appearance features directly associated with shape features, it is necessary to first mine the appearance features directly associated with shape and then use these appearance features to further explore the appearance features indirectly associated with body shape.

So we devised a cascading two-stage attention mechanism that systematically extracts appearance features related to body shape—both directly and indirectly, as shown in Fig.5. The mechanism operates as follows: in the first stage, let the shape feature map  $\tilde{f}_{s,i}$  output by  $F_s$  serve as query, and the appearance feature map  $f_i$  extracted by  $F_a$  serve as key and value:

$$Q = W_q(\tilde{f}_{s,i}), K = W_k(f_i), V = W_v(f_i), \quad (11)$$

Then, similar to ISR, the correlation score between  $Q$  and  $K$  is used to search features directly related to shape in  $V$ , and fused with shape feature map  $\tilde{f}_{s,i}$  to obtain  $\tilde{f}_i^{fuse}$ .

$$\tilde{f}_i^{fuse} = W_{v2}(BN(Norm(QK^T)V)) + \tilde{f}_{s,i}, \quad (12)$$

Considering  $\tilde{f}_i^{fuse}$  contains shape discriminative information and appearance discriminative information directly related to body shape,  $\tilde{f}_i^{fuse}$  can be effectively employed as a query during the second stage of attention, which facilitates the acquisition of appearance features that are both directly and indirectly associated with the body shape. As the query feature of the second-stage attention,  $\tilde{f}_i^{fuse}$  plays a pivotal role in determining whether modality-invariant identity-discriminative features, both directly and indirectly associated with shape, can be effectively extracted from the appearance features. To ensure the discriminability of the query  $\tilde{f}_i^{fuse}$ , we also employ CE loss and WRT loss to jointly constrain  $GeM(\tilde{f}_i^{fuse})$ ,  $GeM$  represents the GeM pooling layer.

$$L_{id}^q = -\frac{1}{n_b} \sum_{i=1}^{n_b} q_i \log(W_{id}^q(GeM(\tilde{f}_i^{fuse}))), \quad (13)$$

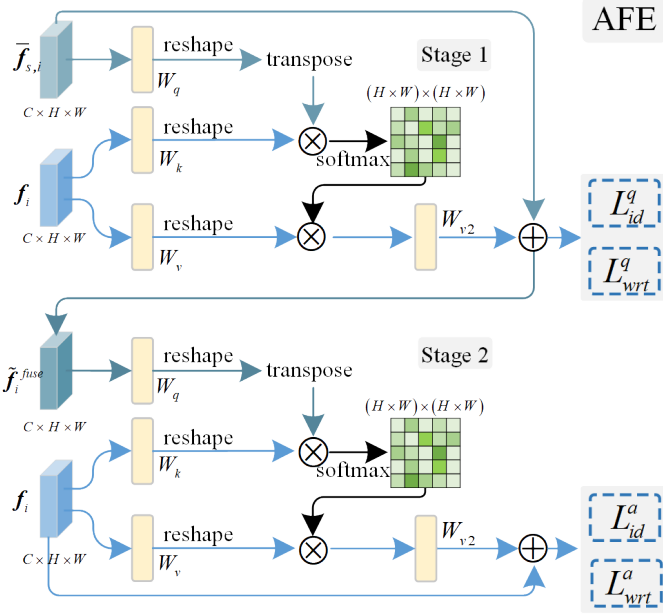


Fig. 5. Illustration of our proposed AFE, it can mine shape-centered appearance features guided by shape features.

where  $W_{id}^q$  represents the shared identity classifier for infrared and visible pedestrian query features.

$$L_{wrt}^q = \frac{1}{n_b} \sum_{i=1}^{n_b} \log(1 + \exp(\sum_{i,j} w_{i,j}^{q,p} d_{i,j}^{q,p} - \sum_{i,k} w_{i,k}^{q,n} d_{i,k}^{q,n})), \quad (14)$$

$$w_{i,j}^{q,p} = \frac{\exp(d_{i,j}^{q,p})}{\sum_{d_{i,j} \in P_i^q} \exp(d_{i,j}^{q,p})}, w_{i,k}^{q,n} = \frac{\exp(-d_{i,k}^{q,n})}{\sum_{d_{i,k} \in N_i^q} \exp(-d_{i,k}^{q,n})}$$

where  $j, k (P_i^q, N_i^q)$  represents the index of the positive and negative samples(set) corresponding to the anchor shape feature  $\tilde{f}_{s,i}$  within a batch size, respectively. And  $d_{i,j}^q$  represents the euclidean distance between two query features:  $d_{i,j}^q = \|(GeM(\tilde{f}_i^{fuse}) - (GeM(\tilde{f}_j^{fuse}))\|_2$ .

In the second stage, we employed the output feature  $\tilde{f}_i^{fuse}$  of the attention of the first stage as a query to emphasize the appearance features directly and indirectly related to the body shape in  $V$  as follows:

$$\tilde{f}_i = W_{v2}(BN(Norm(W_q(\tilde{f}_i^{fuse})K^T)V)) + f_i, \quad (15)$$

Similar to the baseline method, we also utilized a combination of CE loss and WRT loss to jointly constrain appearance features  $GeM(\tilde{f}_i)$  that are closely linked to shape. This constraint serves to enhance their identity discrimination and modality invariance. As follows:

$$L_{id}^a = -\frac{1}{n_b} \sum_{i=1}^{n_b} q_i \log(W_{id}(GeM(\tilde{f}_i))) \quad , \quad (16)$$

$$L_{wrt}^a = \frac{1}{n_b} \sum_{i=1}^{n_b} \log(1 + \exp(\sum_{i,j} w_{i,j}^{a,p} d_{i,j}^{a,p} - \sum_{i,k} w_{i,k}^{a,n} d_{i,k}^{a,n})), \quad (17)$$

$$w_{i,j}^{a,p} = \frac{\exp(d_{i,j}^{a,p})}{\sum_{d_{i,j} \in P_i^a} \exp(d_{i,j}^{a,p})}, w_{i,k}^{a,n} = \frac{\exp(-d_{i,k}^{a,n})}{\sum_{d_{i,k} \in N_i^a} \exp(-d_{i,k}^{a,n})}$$

### Algorithm 1 Training process of the proposed ScRL

**Require:** A mini-batch that consists of  $n_b$  visible(infrared) images  $x_i^{vis}(x_i^{ir})$  and visible(infrared) shapes  $x_{s,i}^{vis}(x_{s,i}^{ir})$ .

**Ensure:** Trained ScRL model.

- 1: **for**  $i = 1; i < iteration; i++$  **do**
- 2: Extract  $\tilde{f}_i^{ir,j}, f_i$  by inputting  $x_i^{vis}, x_i^{ir}$  into the appearance stream network  $F_a$ .
- 3: Extract  $\tilde{f}_{i,s}^{ir,j}$  by inputting  $x_{i,s}^{vis}, x_{i,s}^{ir}$  into the shape stream network  $F_s$ .
- 4: Send  $\tilde{f}_i^{ir,j}, \tilde{f}_{i,s}^{ir,j}$  to the ISR module to obtain the repaired infrared shape feature  $\hat{f}_{s,i}^{ir,j}$ .
- 5: Send  $\hat{f}_{s,i}^{ir,j}$  to the subsequent network of the shape flow  $F_s$  to obtain the final shape features  $\hat{f}_{s,i}$ .
- 6: Extract  $\tilde{f}_{s,i}$  by feeding the output features of the third block of  $F_a$  into the shape subnetwork  $F_s$ .
- 7: Transfer the capability to extract shape features from the shape stream network  $F_s$  to the appearance stream network  $F_a, F_s$  by the SFP module.
- 8: Extract appearance features  $\tilde{f}_i^{fuse}$  directly related to body shape by inputting  $\tilde{f}_{s,i}, f_i$  into stage 1 of the AFE module.
- 9: Extract appearance features  $\tilde{f}_i$  both directly and indirectly related to body shape by inputting  $\tilde{f}_i^{fuse}, f_i$  into stage 2 of the AFE module.
- 10: Optimize  $F_a, F_s, F_s, ISR$  module and AFE module through loss functions  $L_{kd}$ (Eq.7),  $L_{kd_{ce}}$  (Eq.8),  $L_{kd}$ (Eq.9),  $L_{kd_{ce}}$  (Eq.10),  $L_{id}^q$ (Eq.13),  $L_{wrt}^q$ (Eq.14),  $L_{id}^a$ (Eq.16) and  $L_{wrt}^a$ (Eq.17).
- 11: **end for**

where  $j, k (P_i^a, N_i^a)$  represents the index of the positive and negative samples(set) corresponding to the anchor shape feature  $\tilde{f}_i$  within a batch size, respectively. And  $d_{i,j}^a$  represents the euclidean distance between two features:  $d_{i,j}^a = \|(GeM(\tilde{f}_i) - GeM(\tilde{f}_j))\|_2$ .

### D. Training and Inference

In the training process, we employ the appearance flow network  $F_a$  for extracting appearance features and the shape flow network  $F_s$  for extracting shape features. To further enhance this process, we introduce the ISR module to reconstitute inaccuracies in infrared shape features. Additionally, the SFP module is integrated to impart the shape feature extraction capabilities of the shape stream network  $F_s$  to the appearance stream network  $F_a$ . Lastly, the AFE module is introduced to mine appearance features that have both direct and indirect associations with the shape features. The complete training process is executed in an end-to-end fashion, as illustrated in Algorithm 1.

During the testing process, we solely utilize the appearance stream network  $F_a, F_s$  and the AFE module, without involving the shape stream network  $F_s$  and the human parsing network SCHP.

TABLE I  
THE SETTINGS OF DIFFERENT INFRARED VISIBLE RE-ID DATASETS.

Datasets	Type	#Identities	#RGB cam.	#IR cam.	#Images&BBoxes	#Tracklets	#Evaluation
SYSU-MM01 [15]	Image	412	1	1	8240	-	CMC+mAP
RegDB [49]	Image	491	4	2	303420	-	CMC+mAP
HITSZ-VCM [50]	Video	927	12	12	463259	21863	CMC+mAP

TABLE II  
RESULTS OF MAP AND CMC (%) OBTAINED BY OUR PROPOSED METHOD AND THE STATE-OF-THE-ART RE-ID METHODS ON SYSU-MM01. ‘R1’, ‘R10’ AND ‘R20’ DENOTE RANK-1, RANK-10 AND RANK-20, RESPECTIVELY. THESE RESULTS ARE COPIED FROM THEIR PAPERS.

Methods	Reference	<i>All search</i>					<i>Indoor search</i>				
		R1	R10	R20	mAP	mINP	R1	R10	R20	mAP	mINP
Zero-Pad [15]	ICCV’2017	14.8	54.1	71.3	16.0	-	20.6	68.4	85.8	26.9	-
HCML [51]	AAAI’2018	14.3	53.2	69.2	16.2	-	24.5	73.3	86.7	30.1	-
HSME [31]	AAAI’2019	20.7	32.7	78.0	23.1	-	-	-	-	-	-
D <sup>2</sup> RL [36]	CVPR’2019	28.9	70.6	82.4	29.2	-	-	-	-	-	-
eBDTR [52]	TIFS’2019	27.8	67.3	81.3	28.4	-	32.5	77.4	89.6	42.5	-
X-Modal [37]	AAAI’2020	49.9	89.8	96.0	50.7	-	-	-	-	-	-
Hi-CMD [53]	CVPR’2020	34.9	77.6	-	35.9	-	-	-	-	-	-
DDAG [54]	ECCV’2020	54.8	90.4	95.8	53.0	39.6	61.0	94.1	98.4	68.0	62.6
HAT [55]	TIFS’2021	55.3	92.1	97.4	53.9	-	62.1	95.8	99.2	69.4	-
MCLNet [56]	ICCV’2021	65.4	93.3	97.1	62.0	-	72.6	96.9	99.2	76.6	-
CM-NAS [57]	CVPR’2021	62.0	92.9	97.3	60.0	-	67.0	97.0	99.3	73.0	-
MPANet [34]	CVPR’2021	70.6	96.2	98.8	68.2	-	76.7	98.2	99.6	81.0	-
CAJ [47]	ICCV’2021	69.9	95.7	98.5	66.9	-	76.3	97.9	99.5	80.4	-
AGW [3]	TPAMI’2022	47.5	84.4	92.1	47.7	35.3	54.2	91.1	96.0	63.0	59.2
FMCNet [58]	CVPR’2022	66.3	-	-	62.5	-	68.2	-	-	74.1	-
CMMTL [18]	PR’2022	67.3	95.4	98.5	64.3	-	69.6	96.7	99.0	74.4	-
PMT [59]	AAAI’2022	67.5	95.4	98.6	65.0	<u>51.9</u>	71.7	96.7	99.3	76.5	<u>72.7</u>
DSCNet [60]	TIFS’2022	73.9	96.3	98.8	69.5	-	79.4	98.3	99.8	82.7	-
MRCN [33]	AAAI’2023	68.9	95.2	98.4	65.5	-	76.0	<u>98.3</u>	<u>99.7</u>	79.8	-
DEEN [35]	CVPR’2023	74.7	<b>97.6</b>	<u>99.2</u>	71.8	-	<u>80.3</u>	<b>99.0</b>	<b>99.8</b>	83.3	-
SEFL [19]	CVPR’2023	<u>75.2</u>	<u>96.9</u>	99.1	70.1	-	78.4	97.5	98.9	81.2	-
<b>ScRLL(our)</b>		<b>76.1</b>	<b>97.6</b>	<b>99.4</b>	<b>72.6</b>	<b>59.8</b>	<b>82.4</b>	98.8	<b>99.8</b>	<b>85.4</b>	<b>82.2</b>

#### IV. EXPERIMENTS

##### A. Datasets

**SYSU-MM01** [15] is a large-scale dataset with complex environments. The training set consists of 11909 IR (22258 VIS) images of 395 identities captured across 2 IR (4 VIS) cameras. For the testing set, there are 96 pedestrians, with a total of 3,803 IR pedestrian images and 301 randomly selected VIS images.

**RegDB** [49] is a small dataset consisting of 8420 images of 421 identities captured by a single VIS(IR) camera. Each pedestrian has 10 VIS(IR) images. We followed BDTR [61] and randomly divided the dataset into training and testing sets for training and evaluation.

**HITSZ-VCM** [50] is a video-based VI-ReID dataset that contains 251452 VIS images and 211807 IR images of 927 identities, with each track containing 24 consecutive images. The training(testing) set encompasses 11061(10802) tracks of 500(427) identities.

**Evaluation Metrics** We employ Cumulative Matching Characteristics (CMC), mean Average Precision (mAP), and mean Inverse Negative Penalty (mINP) [3] as evaluation metrics to assess the performance of the ScRLL and the methods compared in this paper.

##### B. Implementation Details

Similar to DEEN [35], we adopted ResNet50 pre-trained on imagenet as the backbone and replaced the average pooling layer with the GEM pooling layer, with all input image sizes resized to  $384 \times 144$ . In the training phase, we adopted Random Crop, Random Horizontal Flip, Channel Random Erasing and Channel AdapGray [47] to enhance the IR(VIS) images, and we adopt Random Crop and Random Horizontal Flip for the shape image. We adopt the Adam optimizer for optimization, the learning rate of the classifier  $W_s$ ,  $W_a$  was set to 0.0007, and the learning rate of other networks was set to 0.00035. The model trained a total of 120 epochs, in the first 10 epochs, the learning rate is dynamically adjusted through the warmup strategy, in the 40th and 60th epochs, the learning rate decreases by 10%. At every batch size, we randomly sample 64 images from 8 identities, with 4 VIS (IR) images for each identity and we follow the sampling settings of MITML for HITSZ-VCM [50].

##### C. Comparison with State-of-the-Art Methods

In this section, we present a comprehensive comparison between the proposed ScRLL and other state-of-the-art methods across the SYSU-MM01, RegDB, and HITSZ-VCM datasets. Specifically, the state of the art methods we compared include Zero-Pad [15], HCML [51], HSME [31], D<sup>2</sup>RL [36], eBDTR

TABLE III

RESULTS OF MAP AND CMC (%) OBTAINED BY OUR PROPOSED METHOD AND THE STATE-OF-THE-ART RE-ID METHODS ON REGDB. ‘R1’, ‘R10’ AND ‘R20’ DENOTE RANK-1, RANK-10 AND RANK-20, RESPECTIVELY. THESE RESULTS ARE COPIED FROM THEIR PAPERS.

Methods	Reference	<i>Visible to Infrared</i>					<i>Infrared to Visible</i>				
		R1	R10	R20	mAP	mINP	R1	R10	R20	mAP	mINP
Zero-Pad [15]	ICCV’2017	17.8	34.2	44.4	18.9	-	16.6	34.7	44.3	17.8	-
HCML [51]	AAAI’2018	24.4	47.5	56.8	20.1	-	21.7	45.0	55.6	22.2	-
HSME [31]	AAAI’2019	50.9	73.4	81.7	47.0	-	50.2	72.4	81.1	46.2	-
D <sup>2</sup> RL [36]	CVPR’2019	43.4	66.1	76.3	44.1	-	-	-	-	-	-
eBDTR [52]	TIFS’2019	34.6	59.0	68.7	33.5	-	34.2	58.7	68.6	32.5	-
XModal [37]	AAAI’2020	62.2	83.1	91.7	60.2	-	-	-	-	-	-
Hi-CMD [53]	CVPR’2020	70.9	86.4	-	66.0	-	-	-	-	-	-
DDAG [54]	ECCV’2020	69.3	86.2	91.5	63.5	49.2	68.1	85.2	90.3	61.8	48.6
HAT [55]	TIFS’2021	71.8	87.2	92.2	67.6	-	70.0	86.5	91.6	66.3	-
MCLNet [56]	ICCV’2021	80.3	92.7	96.0	73.1	57.3	75.9	90.9	94.6	69.5	52.6
CM-NAS [57]	ICCV’2021	84.5	95.2	97.9	80.3	-	82.6	94.5	97.4	78.3	-
MPANet [34]	CVPR’2021	83.7	-	-	80.9	-	82.8	-	-	80.7	-
CAJ [47]	ICCV’2021	85.0	95.5	97.5	79.1	65.3	84.8	95.3	97.5	77.8	61.6
AGW [3]	TPAMI’2022	70.1	86.2	91.6	66.4	50.2	70.5	87.2	91.8	65.9	51.2
FMCNet [58]	CVPR’2022	89.1	-	-	84.4	-	88.4	-	-	83.9	-
CMMTL [18]	PR’2022	89.9	96.6	98.3	85.6	-	88.3	96.2	98.0	84.1	-
PMT [59]	AAAI’2022	84.8	-	-	76.6	-	84.2	-	-	75.1	-
DSCNet [60]	TIFS’2022	85.4	-	-	77.3	-	83.5	9-	-	75.2	-
MRCN [33]	AAAI’2023	91.4	98.0	99.0	84.6	-	88.3	96.7	98.5	81.9	-
DEEN [35]	CVPR’2023	91.1	97.8	98.9	85.1	-	89.5	96.8	98.4	83.4	-
SEFL [19]	CVPR’2023	92.2	-	-	86.6	-	91.1	-	-	85.2	-
<b>ScRL(our)</b>		<b>92.4</b>	<b>98.1</b>	<b>99.1</b>	<b>86.7</b>	<b>73.6</b>	<b>91.8</b>	<b>98.0</b>	<b>99.1</b>	<b>85.3</b>	<b>70.9</b>

TABLE IV

RESULTS OF MAP AND CMC (%) OBTAINED BY OUR PROPOSED METHOD AND THE STATE-OF-THE-ART RE-ID METHODS ON HITSZ-VCM. ‘R1’, ‘R5’ AND ‘R10’ DENOTE RANK-1, RANK-5 AND RANK-10, RESPECTIVELY. THESE RESULTS ARE COPIED FROM THEIR PAPERS.

Strategy	Methods	Reference	<i>Infrared to Visible</i>				<i>Visible to Infrared</i>			
			R1	R5	R10	mAP	R1	R5	R10	mAP
Video	MITML [50]	CVPR’22	63.7	76.9	81.7	45.3	64.5	79.0	83.0	47.7
	IBAN [62]	TCSVT’23	65.0	78.3	83.0	48.8	69.6	81.5	85.4	51.0
	SADSTRM [63]	Arxiv’23	65.3	77.9	82.7	49.5	67.7	80.7	85.1	51.8
Image	Lba [64]	ICCV’21	46.4	65.3	72.2	30.7	49.3	69.3	75.9	32.4
	MPANet [34]	CVPR’21	46.5	63.1	70.5	35.3	50.3	67.3	73.6	37.8
	VSD [65]	CVPR’21	54.5	70.0	76.3	41.2	57.5	73.7	79.4	43.5
	CAJ [47]	ICCV’21	56.6	73.5	79.5	41.5	60.1	74.6	79.9	42.8
	SEFL [19]	CVPR’23	67.7	80.3	84.7	52.3	70.2	82.2	86.1	52.5
	<b>ScRL(our)</b>		<b>71.2</b>	<b>83.2</b>	<b>87.4</b>	<b>52.9</b>	<b>73.3</b>	<b>84.4</b>	<b>87.7</b>	<b>53.0</b>

[52], X-Modal [37], Hi-CMD [53], DDAG [54], HAT [55], MCLNet [56], CM-NAS [57], MPANet [34], CAJ [47], AGW [3], FMCNet [58], CMMTL [18], PMT [59], DSCNet [60], MRCN [33], DEEN [35], SEFL [19].

**SYSU-MM01.** As shown in Tab.II, the proposed method exhibits strong competitiveness on SYSU-MM01, particularly in terms of Rank-1, mAP, and mINP. Specifically, in the “all search” mode, the proposed method attained an accuracy of 76.1%, 72.6%, and 59.8% for the Rank-1, mAP, and mINP indicators, respectively. Similarly, in the “indoor search” mode, the proposed method delivered an accuracy of 82.4%, 85.4%, and 82.2% for the Rank-1, mAP, and mINP indicators, respectively. Furthermore, our method outperforms the suboptimal method by 0.9%(2.1%), 0.8%( 2.1%), and 7.9% (9.5%) on Rank-1, mAP, and mINP in “all search”(“indoor search”) mode, respectively. The results suggest that the proposed method, which focuses on pedestrian features with shape as the central component, effectively mitigates modality changes and enhances the accuracy of cross-modality pedestrian matching.

**RegDB.** As illustrated in Tab. III, the proposed approach has showcased commendable performance even on the limited-scale dataset RegDB. Notably, within the “IR to VIS” mode, our method achieved 91.8% and 85.3% accuracy in Rank-1 and mAP indicators, respectively, and has demonstrated superiority over the suboptimal SEFL approach by 0.7% (0.1%) in terms of Rank-1 (mAP). Similarly, in the “VIS to IR” mode, our method attained an accuracy of 92.4% in Rank-1 and 86.7% in mAP, and our method outperformed SEFL in both Rank-1 and mAP metrics. These experimental results demonstrate that our method also achieves significant effectiveness with small-scale datasets.

**HITSZ-VCM.** To verify the scalability of the proposed method, we conducted experiments on the video-based VI-ReID. Specifically, similar to SEFL, we can obtain sequence-level feature by applying an average pooling layer to the frame level. As showcased in Tab. IV, our method has exhibited superior performance compared to all methods grounded in video (image) strategies and achieved 71.2%(73.3%) and

TABLE V  
ABLATION STUDIES OF THE PROPOSED SCRL. **B**: BASELINE. **S**: SFP. **I**: ISR. **A**: AFE.

Setting	Component			<i>All search</i>					<i>Indoor search</i>				
	S	I	A	R1	R10	R20	mAP	mINP	R1	R10	R20	mAP	mINP
B				70.2	95.7	98.6	66.9	52.9	77.6	97.8	99.5	81.1	77.4
+S	✓			73.6	97.1	99.2	70.0	56.5	79.0	98.2	99.4	82.8	79.4
+I	✓	✓		74.6	97.4	99.3	71.0	57.7	79.4	98.4	99.3	83.2	79.8
+A	✓	✓	✓	76.1	97.6	99.4	72.6	59.8	82.4	98.8	99.8	85.4	82.2

TABLE VI  
ABLATION STUDIES OF THE PROPOSED AFE. **S1**: THE ATTENTION OF STAGE 1. **S2**: THE ATTENTION OF STAGE 2.

Setting	Component		<i>All search</i>					<i>Indoor search</i>				
	S2	S1	R1	R10	R20	mAP	mINP	R1	R5	R10	mAP	mINP
B+S+I			74.6	97.4	99.3	71.0	57.7	79.4	98.4	99.3	83.2	79.8
+S2	✓		75.3	97.6	99.3	71.9	58.9	80.4	98.6	99.7	84.0	80.7
+S1	✓	✓	76.1	97.6	99.4	72.6	59.8	82.4	98.8	99.8	85.4	82.2

TABLE VII  
COMPARISON OF PERFORMANCE AND COMPUTATIONAL COSTS ON DIFFERENT SETTINGS IN THE INFERENCE STAGE. **SETTING 1**: BASELINE. **SETTING 2**: TWO INDEPENDENT NETWORKS EXTRACT SHAPE AND APPEARANCE FEATURES RESPECTIVELY, AND CONCATENATE THE TWO FEATURES FOR INFERENCE. **SETTING 3**: BASELINE + SFP. **SET 4**: THE SCRL. **HP**: HUMAN PARSING NETWORK.

Setting	SYSU-MM01( <i>All search</i> )			Params/M (FLOPs/G)			
	R1	mAP	mINP	HP	$F_s$	$F_a$	Total
1	70.2	66.9	52.9	✗	✗	23.5(6.9)	23.5(6.9)
2	71.9	67.5	52.7	66.6(76.5)	23.5(6.9)	23.5(6.9)	113.6(90.3)
3	73.6	70.0	56.5	HP	$F_s$	$F_a, F_s$	38.5(10.1)
4	76.1	72.6	59.8	✗	✗	38.5(10.1)	38.5(10.1)

52.9%(53.0%) accuracy in Rank-1 and mAP in the “VIS to IR”(“IR to VIS”) mode, respectively. In comparison to the video-based approach, our method has demonstrated superior performance by exceeding the suboptimal SADSTRM approach by 5.9% and 3.4% in terms of Rank-1 and mAP, respectively, within the “IR to VIS” mode. Additionally, our method has also outperformed the suboptimal IBAN approach by 3.7% and 2% in terms of Rank-1 and mAP in the “VIS to IR” mode. Furthermore, when compared to the image-based approach, our method has achieved remarkable results in the “VIS to IR”(“IR to VIS”) mode, surpassing the suboptimal SEFL approach by 3.5% (3.1%) in Rank-1 and 0.6% (0.5%) in mAP. The experimental results suggest that our method can extract shape-centered features that remain insensitive to modality variations at the frame level, ensuring robustness in pedestrian feature representation at the sequence level. As a result, it achieves the best performance.

The comparative experimental results have confirmed the effectiveness and advancements of our method for image-based VI-Reid tasks on both the large-scale dataset SYSU-MM01 and the small-scale dataset RegDB. Moreover, our method has demonstrated its effectiveness and advancements in video-based VI-Reid tasks on the large-scale video dataset MITML. These findings underscore the significance of learning shape-centered features, offering tangible benefits for cross-modality pedestrian retrieval.

#### D. Ablation Studies

In this subsection, we analyze the contribution of different components including SFP (Shape Feature Propagation),

ISR (Infrared Shape Restitution), AFE (Appearance Feature Enhancement) based on the SYSU-MM01 dataset.

**Effectiveness of SFP.** To verify the effectiveness of SFP, we integrated the SFP into the Baseline, resulting in “B+S”. This augmentation empowers the model to autonomously acquire shape features from the original image during inference, eliminating the need for shape feature learning and human parsing networks. Specifically, as shown in Tab. V, in “All search”(“Indoor search”) mode, “B+S” has demonstrated improvements of 3.4%(1.4%) in Rank-1, 3.1%(1.7%) in mAP, and 3.6%(2.0%) in mINP when contrasted with the Baseline. These improvements are attributed to the fact that shape features, which remain unaffected by modality changes, complement appearance features, thereby enhancing the overall performance.

Furthermore, we conducted comprehensive experiments on both model and computational complexity. As shown in Tab. VII, we validated the complementarity of shape features to appearance features through experiments in Setting 2, specifically, we utilized two independent networks to extract shape and appearance features and then concatenated these two features for inference. Compared to the Baseline, the Rank-1 (mAP) of Setting 2 increased by 1.7% (0.6%) by increasing the model parameter (computational complexity) by 90.1M (83.4G). In contrast, “B+S” (Setting 3) achieved an even greater improvement of 3.4% in Rank-1 (and 3.1% in mAP) with a relatively modest increment of 15M parameters and 3.2G in computational complexity. This suggests that propagating shape features to the appearance stream network can enhance the acquisition of shape-related features, thus



Fig. 6. Retrieval results under different ablation settings on SYSU-MM01. a, b, c, and d denote “B”, “B+S”, “B+S+I”, and “B+S+I+A”, respectively. The green (red) border represents the same (different) identity. It is evident that the incorporation of various modules has led to a notable enhancement in the hit rate for pedestrian retrieval.

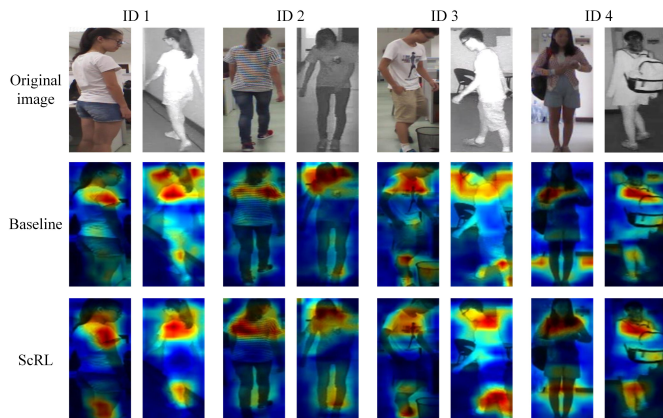


Fig. 7. Visualization of regions that the model interests. The first row depicts the original input pedestrian images, with four pedestrians, each having both an infrared and a visible image. The second row illustrates the region where the Baseline method captures features, while the third row showcases the region where the proposed ScRL method captures features. It’s evident that the ScRL method outperforms the Baseline significantly in capturing these features.

improving the model’s performance. In comparison to Setting 2, The introduction of SFP has also reduced the computational complexity of the inference process, as it eliminates the need for the involvement of shape stream networks and human parsing networks.

**Effectiveness of ISR.** Incorporating SFP extends the shape stream’s capabilities to the appearance stream. However, the incorrect IR shape restricts the potential of the shape stream, subsequently curbing the efficacy of the appearance stream. To tackle this challenge, ISR was introduced to the “B+S”, yielding “B+S+I”. As highlighted in Tab. V, the Rank-1, mAP, and mINP metrics have collectively improved by 1.0%(0.4%),

1.0%(0.4%), and 1.2%(0.4%) in “All search”(“Indoor search”) mode respectively. The performance improvement suggests the feasibility of extracting pertinent information for repairing infrared shape features from the intermediate features of the appearance stream network and underscores ISR’s prowess in restituting inaccurate IR shapes.

**Effectiveness of AFE.** In order to accentuate appearance features linked with shape, we incorporated the AFE into the “B+S+I”. The corresponding results, as depicted in Tab. V, reflect an enhancement in Rank-1, mAP, and mINP, in “All search” mode, these metrics increased from 74.6%, 71.0%, and 57.7% to 76.1%, 72.6%, and 59.8%, respectively, in “Indoor search” mode, the metrics improved from 79.4%, 83.2%, and 79.8% to 82.4%, 85.4%, and 82.2%, respectively. This suggests that in contrast to typical appearance features, appearance features centered on shape are better at emphasizing identity-discriminative information related to individuals while minimizing the influence of background and other irrelevant noise features. Furthermore, as delineated in Tab. VII, the computational overhead imposed by AFE is negligibly minimal after rounding, rendering it inconsequential during the inference phase. This ensures that the introduction of AFE hardly imposes any burden on the model’s inference process.

AFE effectively learns appearance features that have both direct and indirect connections to shape. To confirm its ability to capture features directly associated with shape, we replaced the original query feature of Stage 2 (S2) with shape features. The results in Table VI show that adding S2 to “B+S+I” to create “B+S+I+S2” resulted in improvements across Rank-1, mAP, and mINP. Specifically, when compared to “B+S+I,” there were increases of 0.7%(1.0%), 0.9%(0.8%), and 1.2%(0.9%) in “All search”(“Indoor search”) mode, respectively. Furthermore, when incorporating S1 into the

“B+S+I+S2” configuration to create “B+S+I+S2+S1,” the metrics exhibited further improvements. In the “All search” mode, Rank-1, mAP, and mINP increased from 75.3%, 71.9%, and 58.9% to 76.1%, 72.6%, and 59.8%, respectively. Similarly, in the “Indoor search” mode, the metrics improved from 80.4%, 84.0%, and 80.7% to 82.4%, 85.4%, and 82.2%, respectively. The experimental results affirm that the strategy of initially learning appearance features directly associated with shape and subsequently those indirectly linked is effective. This is due to the fact that appearance features, whether directly or indirectly connected to shape, are modality-insensitive discriminative features pertaining to human subjects.

### E. Visualization

This section encompasses visualization experiments on retrieval results and model interest.

**Retrieval result.** In order to further analyze the effectiveness of different ablation settings, as shown in Fig. 6, we visualized the retrieval results of different ablation settings. Moving left to right, the degree of similarity with the query image progressively decreases. Compared to the Baseline, it is clear that the addition of each module yields improvements in retrieval performance.

**Model interest.** The proposed ScRL primarily learns modality-invariant pedestrian feature representations with a focus on shape. To illustrate the advantages of our method more vividly, we have visualized the heatmap, as displayed in Fig. 7. It is evident that, in comparison to the Baseline method, the proposed ScRL excels in emphasizing more discriminative information about the human body area. Furthermore, it effectively suppresses interference stemming from background noise. This is evident in Fig. 7, where the baseline method concentrates on background objects (the trash cans in column 5 of Fig. 7, as well as the patterns on the wall in column 6, etc), whereas our proposed method exclusively emphasizes the body area.

## V. CONCLUSION AND FUTURE WORKS

This paper introduces the innovative ScRL framework designed to enhance the effective utilization of body shape in VI-ReID. Firstly, we introduce Shape Feature Propagation (SFP), which directly extracts shape features from visible(infrared) pedestrian images. The distinctive characteristic of SFP lies in its ability to avoid the need for the auxiliary model, resulting in a significant reduction in computational complexity. Additionally, the proposed Infrared Shape Restitution (ISR) restitutes errors in the infrared shape at the feature level. This correction enhances the discriminative capacity of infrared shape features. Furthermore, we present the Appearance Feature Enhancement (AFE), which focuses on learning shape-centered appearance features while concurrently suppressing irrelevant identity-unrelated information. The synergy of these techniques culminates in the ScRL framework. Extensive experiments have validated the superiority of ScRL on the SYSU-MM01, RegDB image datasets, and HITSZ-VCM video datasets.

Nonetheless, our proposed method has not taken into account the significant variations in shape features arising from different camera perspectives. This oversight may result in inadequate discrimination of shape features, subsequently impacting the learning of appearance features related to shape, especially when dealing with modality changes. Therefore, in future research, we will delve deeper into the exploration of methods for learning camera-invariant shape features, with the ultimate goal of enhancing the learning of appearance features related to shape.

## REFERENCES

- [1] Y. Sun, L. Zheng, Y. Yang, Q. Tian, and S. Wang, “Beyond part models: Person retrieval with refined part pooling (and a strong convolutional baseline),” in *Proceedings of the European Conference on Computer Vision (ECCV)*, September 2018.
- [2] H. Luo, Y. Gu, X. Liao, S. Lai, and W. Jiang, “Bag of tricks and a strong baseline for deep person re-identification,” in *Proceedings of the IEEE/CVF Conference on Computer Vision and Pattern Recognition (CVPR) Workshops*, June 2019.
- [3] M. Ye, J. Shen, G. Lin, T. Xiang, L. Shao, and S. C. H. Hoi, “Deep learning for person re-identification: A survey and outlook,” *IEEE Transactions on Pattern Analysis and Machine Intelligence*, vol. 44, no. 6, pp. 2872–2893, 2022.
- [4] S. He, H. Luo, P. Wang, F. Wang, H. Li, and W. Jiang, “Transreid: Transformer-based object re-identification,” in *Proceedings of the IEEE/CVF International Conference on Computer Vision (ICCV)*, October 2021, pp. 15 013–15 022.
- [5] H. Tang, J. Liu, S. Yan, R. Yan, Z. Li, and J. Tang, “M<sup>3</sup>net: Multi-view encoding, matching, and fusion for few-shot fine-grained action recognition,” in *ACM international conference on Multimedia (MM)*, 2023.
- [6] N. Dong, L. Zhang, S. Yan, H. Tang, and J. Tang, “Erasing, transforming, and noising defense network for occluded person re-identification,” *arXiv*, 2023.
- [7] H. Li, S. Yan, Z. Yu, and D. Tao, “Attribute-identity embedding and self-supervised learning for scalable person re-identification,” *IEEE Transactions on Circuits and Systems for Video Technology*, vol. 30, no. 10, pp. 3472–3485, 2019.
- [8] S. Yan, H. Tang, L. Zhang, and J. Tang, “Image-specific information suppression and implicit local alignment for text-based person search,” *IEEE Transactions on Neural Networks and Learning Systems*, pp. 1–14, 2023.
- [9] S. Yan, N. Dong, J. Liu, L. Zhang, and J. Tang, “Learning comprehensive representations with richer self for text-to-image person re-identification,” in *ACM international conference on Multimedia (MM)*, 2023.
- [10] S. Yan, Y. Zhang, M. Xie, D. Zhang, and Z. Yu, “Cross-domain person re-identification with pose-invariant feature decomposition and hypergraph structure alignment,” *Neurocomputing*, vol. 467, pp. 229–241, 2022.
- [11] S. Yan, N. Dong, L. Zhang, and J. Tang, “Clip-driven fine-grained text-image person re-identification,” *arXiv*, 2022.
- [12] Y. Wang, G. Qi, S. Li, Y. Chai, and H. Li, “Body part-level domain alignment for domain-adaptive person re-identification with transformer framework,” *IEEE Transactions on Information Forensics and Security*, vol. 17, pp. 3321–3334, 2022.
- [13] Y. Zhang, Y. Wang, H. Li, and S. Li, “Cross-compatible embedding and semantic consistent feature construction for sketch re-identification,” in *Proceedings of the 30th ACM International Conference on Multimedia*, 2022, pp. 3347–3355.
- [14] S. Li, F. Li, J. Li, H. Li, B. Zhang, D. Tao, and X. Gao, “Logical relation inference and multiview information interaction for domain adaptation person re-identification,” *IEEE Transactions on Neural Networks and Learning Systems*, 2023.
- [15] A. Wu, W.-S. Zheng, H.-X. Yu, S. Gong, and J. Lai, “Rgb-infrared cross-modality person re-identification,” in *Proceedings of the IEEE international conference on computer vision*, 2017, pp. 5380–5389.
- [16] B. Yang, M. Ye, J. Chen, and Z. Wu, “Augmented dual-contrastive aggregation learning for unsupervised visible-infrared person re-identification,” in *ACM MM*, 2022, p. 2843–2851.

- [17] B. Yang, J. Chen, X. Ma, and M. Ye, "Translation, association and augmentation: Learning cross-modality re-identification from single-modality annotation," *IEEE Transactions on Image Processing*, vol. 32, pp. 5099–5113, 2023.
- [18] N. Huang, K. Liu, Y. Liu, Q. Zhang, and J. Han, "Cross-modality person re-identification via multi-task learning," *Pattern Recognition*, vol. 128, p. 108653, 2022.
- [19] J. Feng, A. Wu, and W.-S. Zheng, "Shape-erased feature learning for visible-infrared person re-identification," in *Proceedings of the IEEE/CVF Conference on Computer Vision and Pattern Recognition*, 2023, pp. 22752–22761.
- [20] L. Zheng, L. Shen, L. Tian, S. Wang, J. Wang, and Q. Tian, "Scalable person re-identification: A benchmark," in *Proceedings of the IEEE international conference on computer vision*, 2015, pp. 1116–1124.
- [21] Z. Zheng, L. Zheng, and Y. Yang, "Unlabeled samples generated by gan improve the person re-identification baseline in vitro," in *Proceedings of the IEEE international conference on computer vision*, 2017, pp. 3754–3762.
- [22] L. Wei, S. Zhang, W. Gao, and Q. Tian, "Person transfer gan to bridge domain gap for person re-identification," in *Proceedings of the IEEE conference on computer vision and pattern recognition*, 2018, pp. 79–88.
- [23] A. Hermans, L. Beyler, and B. Leibe, "In defense of the triplet loss for person re-identification," *arXiv preprint arXiv:1703.07737*, 2017.
- [24] Y. Sun, L. Zheng, Y. Yang, Q. Tian, and S. Wang, "Beyond part models: Person retrieval with refined part pooling (and a strong convolutional baseline)," in *Proceedings of the European conference on computer vision (ECCV)*, 2018, pp. 480–496.
- [25] G. Wang, Y. Yuan, X. Chen, J. Li, and X. Zhou, "Learning discriminative features with multiple granularities for person re-identification," in *Proceedings of the 26th ACM international conference on Multimedia*, 2018, pp. 274–282.
- [26] S. He, H. Luo, P. Wang, F. Wang, H. Li, and W. Jiang, "Transreid: Transformer-based object re-identification," in *Proceedings of the IEEE/CVF international conference on computer vision*, 2021, pp. 15 013–15 022.
- [27] Z. Zeng, Z. Wang, Z. Wang, Y. Zheng, Y.-Y. Chuang, and S. Satoh, "Illumination-adaptive person re-identification," *IEEE Transactions on Multimedia*, vol. 22, no. 12, pp. 3064–3074, 2020.
- [28] L. Zheng, Y. Huang, H. Lu, and Y. Yang, "Pose-invariant embedding for deep person re-identification," *IEEE Transactions on Image Processing*, vol. 28, no. 9, pp. 4500–4509, 2019.
- [29] Z. Zhong, L. Zheng, Z. Zheng, S. Li, and Y. Yang, "Camera style adaptation for person re-identification," in *Proceedings of the IEEE conference on computer vision and pattern recognition*, 2018, pp. 5157–5166.
- [30] J.-Y. Zhu, T. Park, P. Isola, and A. A. Efros, "Unpaired image-to-image translation using cycle-consistent adversarial networks," in *Proceedings of the IEEE international conference on computer vision*, 2017, pp. 2223–2232.
- [31] Y. Hao, N. Wang, J. Li, and X. Gao, "Hsme: Hypersphere manifold embedding for visible thermal person re-identification," in *Proceedings of the AAAI conference on artificial intelligence*, vol. 33, no. 01, 2019, pp. 8385–8392.
- [32] D. Cheng, X. Wang, N. Wang, Z. Wang, X. Wang, and X. Gao, "Cross-modality person re-identification with memory-based contrastive embedding," in *Proceedings of the AAAI Conference on Artificial Intelligence*, vol. 37, no. 1, 2023, pp. 425–432.
- [33] Y. Zhang, Y. Yan, J. Li, and H. Wang, "Mrcn: A novel modality restitution and compensation network for visible-infrared person re-identification," *arXiv preprint arXiv:2303.14626*, 2023.
- [34] Q. Wu, P. Dai, J. Chen, C.-W. Lin, Y. Wu, F. Huang, B. Zhong, and R. Ji, "Discover cross-modality nuances for visible-infrared person re-identification," in *Proceedings of the IEEE/CVF Conference on Computer Vision and Pattern Recognition*, 2021, pp. 4330–4339.
- [35] Y. Zhang and H. Wang, "Diverse embedding expansion network and low-light cross-modality benchmark for visible-infrared person re-identification," in *Proceedings of the IEEE/CVF Conference on Computer Vision and Pattern Recognition*, 2023, pp. 2153–2162.
- [36] Z. Wang, Z. Wang, Y. Zheng, Y.-Y. Chuang, and S. Satoh, "Learning to reduce dual-level discrepancy for infrared-visible person re-identification," in *Proceedings of the IEEE/CVF conference on computer vision and pattern recognition*, 2019, pp. 618–626.
- [37] D. Li, X. Wei, X. Hong, and Y. Gong, "Infrared-visible cross-modal person re-identification with an x modality," in *Proceedings of the AAAI conference on artificial intelligence*, vol. 34, no. 04, 2020, pp. 4610–4617.
- [38] Z. Wei, X. Yang, N. Wang, and X. Gao, "Syncretic modality collaborative learning for visible infrared person re-identification," in *Proceedings of the IEEE/CVF International Conference on Computer Vision*, 2021, pp. 225–234.
- [39] M. M. Kalayeh, E. Basaran, M. Gökmen, M. E. Kamasak, and M. Shah, "Human semantic parsing for person re-identification," in *Proceedings of the IEEE conference on computer vision and pattern recognition*, 2018, pp. 1062–1071.
- [40] C. Song, Y. Huang, W. Ouyang, and L. Wang, "Mask-guided contrastive attention model for person re-identification," in *Proceedings of the IEEE conference on computer vision and pattern recognition*, 2018, pp. 1179–1188.
- [41] H. Huang, W. Yang, X. Chen, X. Zhao, K. Huang, J. Lin, G. Huang, and D. Du, "Eanet: Enhancing alignment for cross-domain person re-identification," *arXiv preprint arXiv:1812.11369*, 2018.
- [42] J. Guo, Y. Yuan, L. Huang, C. Zhang, J.-G. Yao, and K. Han, "Beyond human parts: Dual part-aligned representations for person re-identification," in *Proceedings of the IEEE/CVF International Conference on Computer Vision*, 2019, pp. 3642–3651.
- [43] K. Zhu, H. Guo, Z. Liu, M. Tang, and J. Wang, "Identity-guided human semantic parsing for person re-identification," in *Computer Vision—ECCV 2020: 16th European Conference, Glasgow, UK, August 23–28, 2020, Proceedings, Part III 16*. Springer, 2020, pp. 346–363.
- [44] P. Hong, T. Wu, A. Wu, X. Han, and W.-S. Zheng, "Fine-grained shape-appearance mutual learning for cloth-changing person re-identification," in *Proceedings of the IEEE/CVF conference on computer vision and pattern recognition*, 2021, pp. 10513–10522.
- [45] P. Li, Y. Xu, Y. Wei, and Y. Yang, "Self-correction for human parsing," *IEEE Transactions on Pattern Analysis and Machine Intelligence*, vol. 44, no. 6, pp. 3260–3271, 2020.
- [46] M. Ye, J. Shen, G. Lin, T. Xiang, L. Shao, and S. C. Hoi, "Deep learning for person re-identification: A survey and outlook," *IEEE transactions on pattern analysis and machine intelligence*, vol. 44, no. 6, pp. 2872–2893, 2021.
- [47] M. Ye, W. Ruan, B. Du, and M. Z. Shou, "Channel augmented joint learning for visible-infrared recognition," in *Proceedings of the IEEE/CVF International Conference on Computer Vision*, 2021, pp. 13 567–13 576.
- [48] X. Wang, R. Girshick, A. Gupta, and K. He, "Non-local neural networks," in *Proceedings of the IEEE conference on computer vision and pattern recognition*, 2018, pp. 7794–7803.
- [49] D. T. Nguyen, H. G. Hong, K. W. Kim, and K. R. Park, "Person recognition system based on a combination of body images from visible light and thermal cameras," *Sensors*, vol. 17, no. 3, p. 605, 2017.
- [50] X. Lin, J. Li, Z. Ma, H. Li, S. Li, K. Xu, G. Lu, and D. Zhang, "Learning modal-invariant and temporal-memory for video-based visible-infrared person re-identification," in *Proceedings of the IEEE/CVF Conference on Computer Vision and Pattern Recognition (CVPR)*, June 2022, pp. 20 973–20 982.
- [51] M. Ye, X. Lan, J. Li, and P. Yuen, "Hierarchical discriminative learning for visible thermal person re-identification," in *Proceedings of the AAAI conference on artificial intelligence*, vol. 32, no. 1, 2018.
- [52] M. Ye, X. Lan, Z. Wang, and P. C. Yuen, "Bi-directional center-constrained top-ranking for visible thermal person re-identification," *IEEE Transactions on Information Forensics and Security*, vol. 15, pp. 407–419, 2019.
- [53] S. Choi, S. Lee, Y. Kim, T. Kim, and C. Kim, "Hi-cmd: Hierarchical cross-modality disentanglement for visible-infrared person re-identification," in *Proceedings of the IEEE/CVF conference on computer vision and pattern recognition*, 2020, pp. 10 257–10 266.
- [54] M. Ye, J. Shen, D. J. Crandall, L. Shao, and J. Luo, "Dynamic dual-attentive aggregation learning for visible-infrared person re-identification," in *Computer Vision—ECCV 2020: 16th European Conference, Glasgow, UK, August 23–28, 2020, Proceedings, Part XVII 16*. Springer, 2020, pp. 229–247.
- [55] M. Ye, J. Shen, and L. Shao, "Visible-infrared person re-identification via homogeneous augmented tri-modal learning," *IEEE Transactions on Information Forensics and Security*, vol. 16, pp. 728–739, 2020.
- [56] X. Hao, S. Zhao, M. Ye, and J. Shen, "Cross-modality person re-identification via modality confusion and center aggregation," in *Proceedings of the IEEE/CVF International conference on computer vision*, 2021, pp. 16 403–16 412.
- [57] C. Fu, Y. Hu, X. Wu, H. Shi, T. Mei, and R. He, "Cm-nas: Cross-modality neural architecture search for visible-infrared person re-identification," in *Proceedings of the IEEE/CVF International Conference on Computer Vision*, 2021, pp. 11 823–11 832.

- [58] Q. Zhang, C. Lai, J. Liu, N. Huang, and J. Han, "Fmcnet: Feature-level modality compensation for visible-infrared person re-identification," in *Proceedings of the IEEE/CVF Conference on Computer Vision and Pattern Recognition*, 2022, pp. 7349–7358.
- [59] H. Lu, X. Zou, and P. Zhang, "Learning progressive modality-shared transformers for effective visible-infrared person re-identification," in *Proceedings of the AAAI Conference on Artificial Intelligence*, vol. 37, no. 2, 2023, pp. 1835–1843.
- [60] Y. Zhang, Y. Kang, S. Zhao, and J. Shen, "Dual-semantic consistency learning for visible-infrared person re-identification," *IEEE Transactions on Information Forensics and Security*, vol. 18, pp. 1554–1565, 2022.
- [61] M. Ye, Z. Wang, X. Lan, and P. C. Yuen, "Visible thermal person re-identification via dual-constrained top-ranking," in *IJCAI*, vol. 1, 2018, p. 2.
- [62] H. Li, M. Liu, Z. Hu, F. Nie, and Z. Yu, "Intermediary-guided bidirectional spatial-temporal aggregation network for video-based visible-infrared person re-identification," *IEEE Transactions on Circuits and Systems for Video Technology*, 2023.
- [63] H. Li, L. Xu, Y. Zhang, D. Tao, and Z. Yu, "Adversarial self-attack defense and spatial-temporal relation mining for visible-infrared video person re-identification," *arXiv preprint arXiv:2307.03903*, 2023.
- [64] H. Park, S. Lee, J. Lee, and B. Ham, "Learning by aligning: Visible-infrared person re-identification using cross-modal correspondences," in *Proceedings of the IEEE/CVF international conference on computer vision*, 2021, pp. 12 046–12 055.
- [65] X. Tian, Z. Zhang, S. Lin, Y. Qu, Y. Xie, and L. Ma, "Farewell to mutual information: Variational distillation for cross-modal person re-identification," in *Proceedings of the IEEE/CVF Conference on Computer Vision and Pattern Recognition*, 2021, pp. 1522–1531.